



Title	Structure of Human Serum Albumin at a Foam Surface
Author(s)	Enomoto, Kanta; Torisu, Tetsuo; Mizuguchi, Junya et al.
Citation	Journal of Agricultural and Food Chemistry. 2024, 72(15), p. 8774-8783
Version Type	AM
URL	<a href="https://hdl.handle.net/11094/95448">https://hdl.handle.net/11094/95448</a>
rights	This document is the Accepted Manuscript version of a Published Work that appeared in final form in Journal of Agricultural and Food Chemistry, © American Chemical Society after peer review and technical editing by the publisher. To access the final edited and published work see <a href="https://doi.org/10.1021/acs.jafc.3c09357">https://doi.org/10.1021/acs.jafc.3c09357</a> .
Note	

*The University of Osaka Institutional Knowledge Archive : OUKA*

<https://ir.library.osaka-u.ac.jp/>

The University of Osaka

## Structure of human serum albumin at a foam surface

Kanta Enomoto<sup>1</sup>, Tetsuo Torisu<sup>1, \*</sup>, Junya Mizuguchi<sup>1</sup>, Ryosuke Tanoue<sup>1</sup>, and Susumu Uchiyama<sup>1,2, \*</sup>

1. Department of Biotechnology, Graduate School of Engineering, Osaka University, 2-1 Yamadaoka, Suita, Osaka, 565-0871, Japan

2. Exploratory Research Center on Life and Living Systems, National Institutes of Natural Sciences, 5-1 Higashiyama, Myodaiji, Okazaki, Aichi 444-8787, Japan

\*Corresponding author

Address correspondence to: Susumu Uchiyama, Ph.D., Department of Biotechnology, Graduate School of Engineering, Osaka University, 2-1 Yamadaoka, Suita, Osaka 565-0871, Japan, Tel. +81-6-6879-4216, Fax: +81-6-6879-7442, E-mail:

[suchi@bio.eng.osaka-u.ac.jp](mailto:suchi@bio.eng.osaka-u.ac.jp)

Tetsuo Torisu, Ph.D., Department of Biotechnology, Graduate School of Engineering, Osaka University, 2-1 Yamadaoka, Suita, Osaka 565-0871, Japan, Tel. +81-6-6879-4216, Fax: +81-6-6879-7442, E-mail: [tetsuo.torisu@bio.eng.osaka-u.ac.jp](mailto:tetsuo.torisu@bio.eng.osaka-u.ac.jp)

1

2 **ABSTRACT**

3 Proteins can be adsorbed on the air-water interface (AWI), and the structural changes  
4 in proteins at the AWI are closely related with the foaming properties of foods and  
5 beverages. However, how these structural changes in proteins at the AWI occur is not  
6 well understood. We have developed a method for the structural assessment of proteins  
7 in the foam state using hydrogen/deuterium exchange mass spectrometry. Adsorption  
8 sites and structural changes in human serum albumin (HSA) were identified in situ at  
9 peptide-level resolution. The *N*-terminus and the loop (E492–T506), which contains  
10 hydrophobic amino acids, were identified as adsorption sites. Both the structural  
11 flexibility and hydrophobicity were considered to be critical factors for the adsorption of  
12 HSA at the AWI. Structural changes in HSA were observed after more than one minute  
13 of foaming and were spread widely throughout the structure. These structural changes at  
14 the foam AWI were reversible.

15

16 **Keywords:** air-water interface, hydrogen/deuterium exchange mass spectrometry, foam,  
17 protein structure

18

19

20       **Introduction**

21       The air-water interface (AWI) is a hydrophobic interface.<sup>1</sup> Proteins are composed of  
22       both hydrophilic and hydrophobic amino acids and are therefore amphiphilic. Thus,  
23       proteins can be adsorbed to the AWI. Structural changes in proteins at the AWI, which is  
24       also referred to as surface denaturation, can occur after adsorption.<sup>2</sup> Because the  
25       hydrophobic interaction between proteins and the AWI is a main driving force of the  
26       adsorption, hydrophobic residues in the proteins, which were buried in the interior of  
27       molecule, become exposed.<sup>3</sup> Understanding the structural changes of proteins at the AWI  
28       is important for many reasons.<sup>4-6</sup> For example, therapeutic proteins can be adsorbed on  
29       the AWI during the manufacture and storage of biopharmaceuticals, which can result in  
30       changes in the structures of such proteins.<sup>4</sup> These structural changes can lead to the  
31       formation of protein aggregates, which could elicit an immune response; thus, creating a  
32       potential risk for immunogenicity.<sup>7</sup> In addition, understanding the interfacial structural  
33       instability of viruses that can be transmitted by airborne droplets is important for  
34       developing strategies to prevent the spread of viral infections.<sup>1</sup>

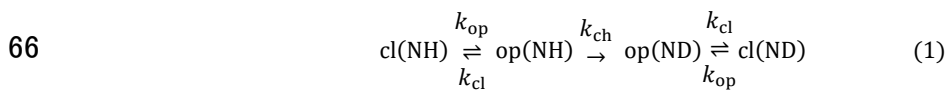
35       Protein adsorption at the AWI is utilized in the food industry, including in producing  
36       meringues, which are made from egg-white proteins that have excellent foaming

37 properties.<sup>8</sup> In addition, foam is a key quality attribute of both sparkling wine and beer,  
38 and proteins play an important role in the formation of the foam of these beverages.<sup>9</sup>  
39 Therefore, many studies have investigated improving the foaming ability, as well as the  
40 foaming stability of foods. Previous studies have demonstrated that the surface  
41 hydrophobicity of proteins was correlated with the foam properties.<sup>10</sup> In addition, having  
42 the molecular flexibility to expose previously buried hydrophobic amino acids to the AWI  
43 has also been indicated to be an important factor for foam formation.<sup>3</sup> The addition of  
44 molecules, such as polyphenols<sup>11,12</sup> and saccharides,<sup>13</sup> and chemical modification, such  
45 as oxidation,<sup>14,15</sup> has been shown to change the protein structure and/or structural  
46 flexibility in solution leading to improvements in the foaming properties. Although these  
47 studies have indicated that the protein structure in the foam state is related to the foam  
48 properties, knowledge of the protein structure in the foam state remains elusive.

49 Analysis of protein structure at the AWI is more challenging than structural analysis  
50 of proteins in solution because signals derived from proteins at the AWI, which are  
51 typically weak because of the limited amount of protein at the AWI, need to be  
52 selectively detected. For this reason, protein structure at the AWI has mainly been  
53 evaluated using spectroscopic and scattering techniques, which provide spectra from  
54 light scattered or reflected from the AWI.<sup>4,16</sup> However, such analytical techniques are

55 only applicable to controlled flat interfaces (e.g., planar interfaces produced by  
56 Langmuir troughs), not to three-dimensional interfaces, such as the foam AWI, because  
57 the angles of incident light and the angles of the detectors for the reflected or scattered  
58 light need to be specific. In addition, the structural resolution of spectroscopic and  
59 solution scattering/reflection techniques is relatively low (secondary structure level),  
60 thus an analytical method with higher structural resolution is desirable.

61 Hydrogen/deuterium exchange mass spectrometry (HDX-MS) can be used to study  
62 protein structures and interactions by monitoring the isotopic exchange of amide  
63 hydrogens with deuterium atoms in the protein backbone after a protein is exposed to  
64 D<sub>2</sub>O.<sup>17</sup> The deuterium exchange of each amide hydrogen in folded proteins can be  
65 expressed by the following equation, the Linderstrøm-Lang model:<sup>18</sup>



67 where cl corresponds to the folded state and op corresponds to the open state, NH and  
68 ND are the protiated and deuterated amides, respectively,  $k_{\text{op}}$  and  $k_{\text{cl}}$  are the rate  
69 constants of the opening and closing reactions, respectively, and  $k_{\text{ch}}$  is the chemical  
70 deuteration rate constant. From this model, the observed deuteration rate constant ( $k_{\text{HD}}$ )  
71 can be obtained:

72 
$$k_{\text{HD}} = \frac{k_{\text{op}} \times k_{\text{ch}}}{k_{\text{op}} + k_{\text{cl}} + k_{\text{ch}}} \quad (2)$$

73 Under stable conditions, proteins can be refolded immediately after the unfolding.<sup>18</sup>

74 Thus,  $k_{cl}$  is much larger than  $k_{op}$  and  $k_{ch}$ , and then  $k_{HD}$  can be simplified as follows:

75 
$$k_{HX} = \frac{k_{op}}{k_{cl}} \times k_{ch} = K_{op} \times k_{ch} \quad (3)$$

76 where  $K_{op}$  is the equilibrium constant of the opening reaction. Amide hydrogens often

77 form hydrogen bonds, which stabilize the protein structure and result in the value for

78  $K_{op}$  being smaller, and thus the exchange of amide hydrogens in a folded protein is

79 slower than that in the unfolded state in which the hydrogen bonds featuring amide

80 hydrogens are partially or completely disrupted.<sup>19</sup> In addition, the accessibility of the

81 protein for the deuterium atoms influences the exchange rate. For example, when an

82 amide hydrogen is buried inside the protein or covered by additives or other proteins,

83 the exchange rate is slower compared with when the hydrogen is on the outside of the

84 protein.<sup>19</sup> In a typical bottom-up HDX-MS measurement, proteolytic digestion of a

85 protein that has been exposed to  $D_2O$  is conducted, followed by liquid chromatography

86 and mass analysis. The deuterium uptake profiles of the resulting peptides provide

87 information on the secondary, tertiary, and higher order structure of the protein at

88 peptide-level resolution,<sup>20</sup> which is a higher resolution compared with that observed

89 with spectroscopic and solution scattering/reflection techniques.

90 Previous studies have demonstrated that HDX-MS can be a valuable technique to  
91 examine protein structures at interfaces.<sup>21-23</sup> Xiao and Konermann have used HDX-MS  
92 to investigate the structural change of myoglobin at the AWI and proposed a surface  
93 denaturation model, although this group did not perform a detailed structural analysis at  
94 peptide-level resolution.<sup>24</sup> Another study has demonstrated that HDX-MS was useful for  
95 evaluating protein structure at a flat AWI.<sup>25</sup> However, the characteristics of the AWI  
96 interface, such as the curvature of the interface and the bulk/interface volume ratio, are  
97 different between flat and foam AWIs, and the protein structure at a flat AWI can be  
98 different from that at a foam AWI. Therefore, a method that can evaluate protein  
99 structure at a foam AWI is needed to reveal the molecular mechanism of protein foam  
100 formation. In the present study, human serum albumin (HSA) was used as a model  
101 protein because HSA can be highly purified and has adequate foaming properties. The  
102 structure of HSA in solution has been well characterized,<sup>26</sup> and the three-dimensional  
103 structure of HSA is similar to that of bovine serum albumin,<sup>27</sup> which is found in foods  
104 such as milk.<sup>28</sup> Thus, HSA can be used as a model protein for application to food  
105 processing. We have developed an in situ method to evaluate the structure of HSA in  
106 the foam state using HDX-MS. Structural information on HSA at the foam AWI was

107 successfully obtained at peptide-level resolution using the developed method. Analysis  
108 after defoaming revealed that the structural changes at the foam AWI were reversible.

109

## 110 **Materials and methods**

### 111 **Materials**

112 HSA and all other reagents were purchased from Fujifilm Wako (Osaka, Japan) unless  
113 otherwise specified. The HSA monomer content, determined by size exclusion  
114 chromatography (SEC) with UV detection at 280 nm, was 50.5%. Phosphate-buffered  
115 saline (1×PBS; pH 7.4) and acetonitrile were obtained from Thermo Fisher Scientific  
116 (Waltham, MA, USA). D<sub>2</sub>O was purchased from Iwatani Corporation (Osaka, Japan).

117

### 118 **Preparation of HSA samples**

119 Prior to analysis, HSA monomer was fractionated by SEC with a HiLoad 16/60  
120 Superdex 200 column (Cytiva, Tokyo, Japan), and 1×PBS at pH 7.4 was used as the  
121 elution buffer. The HSA monomer content was 99.1% after the purification. Fractionated  
122 HSA monomer was dialyzed against 100 mM sodium phosphate buffer at pH 7 at 4°C,  
123 and then concentrated by ultrafiltration using Amicon Ultra 10k (Merck, Darmstadt,  
124 Germany) to 10 mg/mL for circular dichroism (CD) spectroscopy and interfacial tension

125 measurement, 5 mg/mL for HDX-MS measurements in the liquid state, and 100 mg/mL  
126 for HDX-MS measurements in the foam state.

127

## 128 **Interfacial tension measurement**

129 Static surface tension was measured by the Whilhelmy method using a Sigma 700  
130 instrument (Biolin Scientific, Gothenburg, Sweden) equipped with a platinum plate. The  
131 plate was immersed in 10 mg/mL HSA solution to an immersion depth of 6 mm and  
132 pulled up three times at a rate of 20 mm/min. The force (F) that acted on the plate was  
133 measured and the surface tension ( $\gamma$ ) was calculated from the equation:<sup>29</sup>

$$134 \quad \gamma = \frac{F}{L} \quad (4)$$

135 where L is the perimeter of the plate (39.24 mm). The average of three measurements  
136 was reported. Dynamic surface tension was measured by the pendant drop method using  
137 a Theta Flex instrument (Biolin Scientific, Gothenburg, Sweden). In the measurements,  
138 a 10- $\mu$ L pendant drop was generated at a flow rate of 2  $\mu$ L/s, and the shape of the pendant  
139 drop was monitored for 1200 s. The surface tension was simultaneously calculated from  
140 the Young-Laplace equation every 10 s using OneAttension (ver.4.0.3).<sup>30</sup>

141

## 142 **Foaming of HSA**

143 An electric milk frother (GOSCIEN, MFB1501B, Guangzhou, China) was employed  
144 to foam the HSA solution (Fig. 1). The foam was generated quickly by mechanical  
145 agitation created by rotating the frother head made of stainless steel at 15,000 rpm. The  
146 mechanical agitation was continued until just before the analysis.

147

#### 148 **SEC after the foaming**

149 HSA foam was generated for 0, 0.5, 1, 5, 10, 30, 60, and 90 min. At each time point,  
150 the foam was collected and weighed. The weight was divided by the density of the HSA  
151 solution (1.01 g/mL) to calculate the volume of solution contained in the collected foam,  
152 and then the foam was diluted with sodium phosphate buffer with 0.03% silicone  
153 antifoam to achieve a concentration of 1 mg/mL for the samples at all time points. The  
154 samples were centrifuged at  $15,000 \times g$  at 4°C for 30 min. The supernatants were then  
155 loaded onto a ACQUITY UPLC System (Waters, Milford, MA, USA) equipped with a  
156 TSKgel UP-SW3000 column (4.6 mm  $\times$  150 mm; Tosoh Bioscience, Tokyo, Japan).  
157 Isocratic elution was performed using 133 mM phosphate buffer with 200 mM  
158 KCl/acetonitrile (95:5) at a flow rate of 0.25 mL/min for 15 min. UV absorbance at 280  
159 nm was monitored. Empower 3 Software (Waters) was used to calculate the peak areas.

160 The monomer (%) was calculated as a ratio of the monomer area to the total peak area at  
161 each time point. The measurements were performed in triplicate.

162

### 163 **CD spectroscopy after the foaming**

164 To evaluate the secondary structure of HSA before and after the foaming, CD spectra  
165 were obtained using a J-1500 CD spectropolarimeter (Jasco, Tokyo, Japan) equipped with  
166 a Peltier-type temperature controller PTC-510 and PM-539 detector. HSA solution (10  
167 mg/mL) was foamed using the electrical milk frother for 1, 10, 30, and 90 min. The HSA  
168 samples, before and after the foaming, were treated with silicone antifoam and diluted to  
169 0.33  $\mu\text{g/mL}$  with 100 mM phosphate buffer. CD spectra of the samples were collected at  
170 a pathlength of 3 mm in the far UV region (190–260 nm) with a step size of 0.5 nm at  
171 25°C. The spectrum of the blank (100 mM sodium phosphate buffer) was subtracted from  
172 the sample spectra. The observed ellipticity ( $\theta_{obs}$ ) in millidegrees was converted to mean  
173 residue ellipticity (MRE) in  $\text{deg cm}^2 \text{dmol}^{-1}$ , which was calculated from the equation:

$$174 \quad MRE = \frac{\theta_{obs} \times \epsilon_{205}}{10 \times A_{205} \times n} \quad (5)$$

175 where  $n$  is the number of amino acid residues (585 for HSA) and  $\epsilon_{205}$  is the extinction  
176 coefficient at 205 nm. The extinction coefficient of HSA was calculated as 2,199,430  $\text{M}^{-1}$   
177  $\text{cm}^{-1}$  from the protein sequence using the Protein Parameter Calculator.<sup>31</sup>  $A_{205}$  is the

178 absorbance at 205 nm measured using a J-1500 spectropolarimeter. The  $\alpha$ -helix content  
179 was calculated from the signals in the spectra from 200 to 250 nm using BeStSel.<sup>32</sup>

180

## 181 **HDX-MS**

182 HSA solution at 100 mg/mL was foamed using the electrical milk frother immediately  
183 after 10-fold dilution with deuterated buffer (100 mM sodium phosphate buffer, pD 7  
184 with isotope effect correction<sup>33</sup>). The hydrogen/deuterium exchange reaction proceeded  
185 with continuous foaming at 20°C for various time periods: 60; 600; 1800; and 5400 s. A  
186 non-deuterated sample was also prepared by 10-fold dilution with 100 mM sodium  
187 phosphate buffer, pH 7.0. A quenching solution [100 mM NaH<sub>2</sub>PO<sub>4</sub>, 3 M guanidine  
188 hydrochloride (GdnHCl), and 112.5 mM tris (2-carboxyethyl) phosphine hydrochloride]  
189 with 0.025% silicone antifoam was used to defoam the samples and quench the exchange  
190 reaction. A 100- $\mu$ L aliquot of sample in the foam state (approximately 12  $\mu$ L as solution),  
191 which was taken from the foam at a site well above the frothing coil, and 988  $\mu$ L of the  
192 quenching solution were mixed manually at 4°C, and the pH of the mixed solution was  
193 decreased to 2.5. The quenched samples were placed in vials, and subsequent analysis  
194 was conducted automatically using the HDX manager and HDX PAL system (Waters).  
195 Samples (50  $\mu$ L) were injected into HDX manager, and then HSA was digested online by

196 two tandemly connected BEH pepsin columns (2.1 mm × 30 mm; Waters) with 0.1%  
197 formic acid in water at 100 μL/min. The peptic peptides were trapped in a VanGuard  
198 BEH Pre-column (2.1 mm × 5 mm; Waters). The online pepsin digestion and the trapping  
199 were performed in 4 min. The samples were loaded from the pre-column to the separation  
200 column (ACQUITY BEH C18 1.7 μm, 1.0 mm × 100 mm; Waters) and separated with a  
201 9-min linear gradient of acetonitrile containing 0.1% formic acid increasing from 4% to  
202 40% in water containing 0.1% formic acid. The flow rate of the mobile phase was 40  
203 μL/min. Eluted peptides were detected using a SYNAPT G2 mass spectrometer (Waters).  
204 The deuteration rate after the quenching was distinctly low,<sup>18</sup> and thus the resulting mass  
205 of each peptide could be used to reflect the HSA structure at the AWI. The measurements  
206 were performed in triplicate (n = 3).

207 The hydrogen/deuterium exchange rate of HSA was also evaluated in the liquid state  
208 to compare the hydrogen/deuterium exchange rate with that of the foam state. The entire  
209 measurement process was automatically performed by the HDX PAL system. Given the  
210 liquid handling volume of the HDX PAL system, the HSA concentration and quenching  
211 conditions were adjusted to inject the same amount of HSA as for the foam state  
212 measurements. Sample solutions were diluted to 5 mg/mL, and 5 μL of each sample  
213 solution was mixed with 45 μL of deuterated buffer. The mixed solutions were incubated

214 at 20°C for the predetermined hydrogen/deuterium exchange time periods, which were  
215 the same as for the foam state measurements. A quenching solution composed of 150 mM  
216 NaH<sub>2</sub>PO<sub>4</sub>, 4.5 M GdnHCl, 168.75 mM tris (2-carboxyethyl) phosphine hydrochloride,  
217 and 0.03% silicone antifoam was used for the liquid state measurements. In the quenching  
218 step, the pH of the sample solution was decreased to 2.5 by mixing 25 µL of the sample  
219 solution and 75 µL of quenching solution at 4°C. The injection volume, online digestion  
220 conditions, and LC-MS conditions were the same as for the measurements of the foam  
221 state samples. A non-deuterated sample was prepared and analyzed in the same manner  
222 using non-deuterated buffer.

223 Defoamed solution samples were also analyzed. HSA solution (10 mg/mL) was  
224 foamed for 90 min using the electrical milk frother. Then, the sample was defoamed by  
225 1:1 mixing with 0.05% antifoam (the final concentration of the antifoam was 0.025%).  
226 HDX-MS measurements of the defoamed solution samples were conducted in the same  
227 manner as for the liquid state measurements.

228 Peptic peptides detected in the non-deuterated sample were identified using the  
229 ProteinLynx global server 3.0 (Waters), and the retention time and MS spectrum were  
230 used to assign the deuterated peptic peptides. A full deuterated (FD) sample was prepared  
231 by incubating HSA in deuterated phosphate buffer containing 6 M urea (final D<sub>2</sub>O% was

232 98%) for 24 h at room temperature. The back-exchange rate was calculated from the result  
233 for the FD sample. The HDX results were mapped on the HSA crystal structure (PDB ID:  
234 4K2C) using Pymol.

235

236

### 237 **Statistical analysis**

238 Data are expressed as the mean or mean  $\pm$  standard deviation (SD). HSA monomer%  
239 and total peak area obtained by SEC were analyzed with Dunnett's multiple comparison  
240 test using the data without foaming as a control.

241 The statistical analysis of differential HDX measurements was performed based on the  
242 principle of uncertainty propagation.<sup>34</sup> Deuteration differences at each time point ( $\Delta D_t$ )  
243 were calculated as follows:

$$244 \quad \Delta D_t = m_a - m_b \quad (6)$$

245 where  $m_a$  and  $m_b$  correspond to the mean of replicate measurements of the centroid mass  
246 of each peptide in states A and B, i.e., the foam and liquid states or the liquid and  
247 defoamed states. Pooled SD ( $s_p$ ) was also calculated:

$$248 \quad s_p = \sqrt{\frac{\sum s_a^2 + \sum s_b^2}{2 \times n_p \times n_t}} \quad (7)$$

249 where  $S_a$  and  $S_b$  are the standard deviations of replicate measurements of the centroid  
250 mass of each peptide in the two states,  $n_p$  is the number of detected peptides, and  $n_t$  is the  
251 number of time points. The combined uncertainties of  $\Delta D_t$  using the  $s_p$  were calculated  
252 from the following equation:<sup>34</sup>

$$253 \quad u(\Delta D_t) = S_p \sqrt{\frac{2}{n}} \quad (8)$$

254 where  $n$  is the number of replicates ( $n=3$ ). All deuteration difference results were tested  
255 for significance, using the coverage factor  $k = 4.6$ <sup>35</sup> according to

$$256 \quad H_0: |\Delta D_t| \leq k \times u(\Delta D_t) \quad (9)$$

257 where  $H_0$  is the null hypothesis. When  $H_0$  was rejected, the difference in HDX was  
258 considered as significant.

259

260

## 261 **Results and discussion**

### 262 **Adsorption of HSA at the AWI**

263 Surface tension measurements were conducted to determine the adsorption of HSA at  
264 the AWI. The static surface tension values of the HSA solution and phosphate buffer  
265 measured by the Wilhelmy method were  $50.6 \pm 0.16$  and  $70.8 \pm 0.05$  mN/m, respectively

266 (Table S1). The lower surface tension of the HSA solution compared with that of the  
267 phosphate buffer indicated the adsorption of HSA at the AWI.

268 Dynamic surface tension measurements by the pendant drop method were performed  
269 to evaluate the adsorption kinetics of HSA at the AWI. As shown in Fig. 1a, the surface  
270 tension of the HSA solution decreased rapidly and reached a plateau in 600 s at  
271 approximately 52 mN/m, which was slightly higher than the static surface tension  
272 measured by the Wilhelmy method. A certain amount of HSA was adsorbed to the AWI  
273 and formed a dense phase immediately after a clean surface was generated because there  
274 was no time lag in the decrease in the surface tension<sup>3</sup> Considering that the interface/bulk  
275 volume ratio of the foam was much larger than that of the pendant drop, and that the mass  
276 transfer of protein is an important factor in adsorption kinetics,<sup>3</sup> the adsorption of HSA  
277 could be faster than that observed in the dynamic surface tension measurements and could  
278 have occurred in the second timescale, or faster, in the foam state.

279 Different from the foaming of the phosphate buffer, a firm foam was obtained  
280 immediately after the start of the foaming for the HSA solution (Fig. 1b), also suggesting  
281 rapid adsorption of HSA to the foam AWI. Because the following HDX-MS  
282 measurements were performed on the timescale of minutes, the hydrogen/deuterium  
283 (H/D) exchange rates could reflect the HSA structure after the adsorption to the foam

284 AWI. The area of the solid-liquid interface (interface with the glass container) was also  
285 increased by foaming, and the interaction with the solid-liquid interface could have an  
286 influence on the H/D exchange rates. However, as shown in Fig. 1b, the increase in the  
287 solid-liquid interface area was approximately fourfold and this was much smaller than  
288 the increase in the AWI area. Thus, the difference in the H/D exchange rates was likely  
289 to mainly arise from the interaction with the AWI or the structural changes of HSA at the  
290 AWI.

291

## 292 **Aggregation of HSA by foaming**

293 Structural changes at an interface can result in protein aggregation.<sup>36</sup> Because  
294 knowledge of the aggregate distribution is crucial for the correct interpretation of the  
295 HDX-MS results, SEC analysis was performed on the foam samples after the defoaming.  
296 A main peak derived from the monomer was observed at approximately 6 min and the  
297 peaks of aggregates were eluted before the main peak (Fig. 2b). A significant decrease ( $p$   
298  $< 0.01$ ) in monomer% was observed after 90 min of foaming. The area% of aggregates  
299 was 0.9% at 0 min and this was significantly increased to 10.1% at 90 min (Fig. 2a). No  
300 significant differences in the total peak area were observed, suggesting that large  
301 aggregates that could not be analyzed by SEC were not generated by foaming.

302 In a previous study, greater than 30% of the HSA monomer formed aggregates after  
303 foaming by jetting the HSA solution.<sup>37</sup> Although the cause of this difference in the  
304 amount of aggregates generated by foaming in the previous study compared with the  
305 present study might be because of differences in the formulation conditions, there is also  
306 the possibility that foaming using a milk frother could be gentler than foaming by jetting  
307 the protein solution. Foaming using a milk frother could be more suitable for the  
308 evaluation of protein structure at the foam AWI with less influence of aggregation.

309

#### 310 **Structural changes in HSA at the foam AWI**

311 The structure of HSA at the foam AWI was evaluated by a comparison of the H/D  
312 exchange rate between the foam and liquid states. The back exchange rate, uptake plots  
313 for each peptide, and other information recommended by Glenn R. Masson et al.<sup>38</sup> are  
314 summarized in the Supporting Information (Table S2). The H/D exchange rates for 68  
315 peptides, which accounted for 57.4% of the amino acid sequence of HSA, were compared.

316 The deuterium uptake values for each peptide at each time point in the foam and the  
317 liquid states were statistically compared according to the recommendations of David D.  
318 Weis.<sup>34</sup> Significant differences in deuterium uptake were observed for 23 peptides when  
319 the deuterium uptake was compared between the foam and liquid states; 21 peptides

320 showed higher deuterium uptake and 2 peptides showed lower deuterium uptake in the  
321 foam state than in the liquid state (Fig. 3 and S1).

322 Peptides A2-F19 and E492-T506 showed significantly lower deuterium uptake at 1  
323 min in the foam state compared with in the liquid state. Because the level of HSA  
324 aggregates was only slightly increased by foaming for 1 min (Fig. 2), a possible  
325 explanation for the lower deuterium uptake for these two peptides was that when the HSA  
326 molecules were adsorbed to the AWI, the regions containing these two peptides faced to  
327 the air side of the foam AWI.<sup>10</sup> Thus, the adsorption to the AWI resulted in lower  
328 accessibility of deuterium at the adsorption site. These differences in deuterium uptake  
329 had disappeared after 10 min, indicating that the adsorption of the HSA molecule at the  
330 AWI at 1 min was reversible, i.e., an adsorption/desorption process was occurring. The  
331 region that had been protected from H/D exchange was then exposed to the deuterium  
332 when the HSA molecule was desorbed into the bulk solution.<sup>39</sup> The results of dynamic  
333 surface tension measurements showed that HSA was adsorbed on the AWI at 1 min;  
334 however, given that structural changes result in very slow desorption or irreversible  
335 adsorption,<sup>3</sup> the interfacial structural changes were negligible or did not occur at 1 min.  
336 Therefore, there were no significant differences in the H/D exchange rate that could be  
337 related to structural perturbation at 1 min.

338 Peptides with significantly higher deuterium uptakes in the foam state were observed  
339 after 10 min (Fig. 3a). The Linderstrøm-Lang model (Equation 1)<sup>18</sup> indicated that the  
340 peptide regions were in the open state more frequently in the foam state than in the liquid  
341 state. In other words, the structure of the HSA molecule was substantially fluctuating at  
342 the foam AWI. The structural changes occurred over the entire peptide structure. When  
343 fractional deuterium uptake was calculated based on the maximum theoretical mass  
344 change (number of peptide bonds – number of prolines, which do not have an amide  
345 hydrogen), the differences in the fractional uptake were comparable between the peptides  
346 that showed significantly higher deuterium uptake (Fig. S3). This result inferred that the  
347 extent of the structural changes for all of these peptides was equivalent. A previous study  
348 has suggested that the structure of the region surrounding the adsorption site could be  
349 particularly changed.<sup>25</sup> The deuterium uptake of D1-N18 and D1-F19, peptide regions  
350 that have considerable overlap with the adsorption site A2-F19, in the foam state was  
351 significantly higher than that in the liquid state at 90 min (Fig. 3c). The peptide A2-F19  
352 also showed higher deuterium uptake in the foam state at 90 min but the difference from  
353 the liquid state was not statistically significant. These results indicated that the influence  
354 of structural changes at the *N*-terminus on the deuterium uptake could be greater than the  
355 shielding effect of the adsorption to the foam AWI. E492-T506, colored in magenta in

356 Fig. 3c, is another adsorption site and the peptide S480-R521, which includes E492-T506,  
357 showed higher deuterium uptake in the foam state; however, there was no difference in  
358 the deuterium uptake of E492-T506 at 90 min. The peptide E492-T506 forms a loop with  
359 few hydrogen bonds between the main chains, and therefore deuterium exchange in E492-  
360 T506 cannot be used to determine any structural changes because deuterium exchange is  
361 sensitive to changes in hydrogen bonding in secondary structures, such as  $\alpha$ -helix and  $\beta$ -  
362 sheet, in which most of the amides form hydrogen bonds with carbonyl groups.<sup>40,41</sup> Thus,  
363 the difference in the deuterium uptake is likely to be related to structural changes in the  
364 region S480-R521, excluding E492-T506, (i.e., S480-L491 and/or F507-R521).

365 Aggregates of HSA were generated by the foaming and could prevent the deuterium  
366 uptake of peptides located at the interface of the aggregates. Although this aggregation  
367 could lead to an underestimation of the increase in deuterium uptake, and there was a  
368 possibility that some structurally perturbed peptides could be overlooked, we focused  
369 on the peptides that showed significantly higher deuterium exchange rates because these  
370 peptides are likely to be the characteristic peptides that are structurally perturbed by  
371 foaming. Furthermore, the presence of aggregates could lead to an overestimation of the  
372 decrease in deuterium uptake; however, there were no peptides that showed significantly  
373 lower deuterium uptake in the foam state.

374 To the best of our knowledge, this is the first report of the protein adsorption sites and  
375 structural changes at a foam AWI. The method developed here will be useful to elucidate  
376 the molecular mechanisms of protein foam properties from the viewpoint of the peptide  
377 structure at the foam AWI. Protein foam properties can be altered by the presence of other  
378 components, such as polyphenols, in food products.<sup>11,12</sup> While it is difficult to elucidate  
379 the interaction sites and protein structures at a foam AWI in the presence of other  
380 components using conventional methods, the developed method using HDX-MS can  
381 provide insight into the molecular mechanisms of protein foam properties from the  
382 viewpoint of the interaction and structure at the foam AWI.

383

#### 384 **Structure of HSA after defoaming**

385 The secondary structure of HSA before and after defoaming was examined using CD  
386 spectroscopy. The CD spectrum of HSA before foaming showed a helix-specific pattern,  
387 which was consistent with previously reported spectra.<sup>42</sup> The CD spectra after foaming  
388 for 1, 30, 60, and 90 min were measured immediately after defoaming. As shown in Fig.  
389 4, there were no obvious differences in the spectra before and after defoaming. The  
390 secondary structure composition was estimated from each spectrum from 200 to 250 nm  
391 using BeStSel. Consistent with the visual comparison of the CD spectrum, the calculated

392 secondary structure composition was not changed obviously by the foaming and  
393 defoaming. In the HDX-MS measurements, several peptides containing an  $\alpha$ -helix  
394 showed higher deuterium uptake in the foam state after more than 1 min of foaming.  
395 Considering that the hydrogen bonding of amide hydrogens in an  $\alpha$ -helix results in slower  
396 deuterium exchange, structural perturbations in the  $\alpha$ -helix regions would be caused by  
397 the foaming. Although there is a possibility that CD cannot detect the structural changes  
398 or the differences in solvent accessibility detected using HDX-MS because of the  
399 differences in the measurement principles, the CD results after defoaming indicated that  
400 the structural changes in HSA at the AWI are likely to be reversible.

401 To evaluate the reversibility of the structural changes at the AWI caused by foaming,  
402 structural change was induced by foaming for 90 min, and the HDX-MS measurement  
403 was also performed after defoaming of the foamed sample. Eight peptides showed  
404 significant differences in the deuterium uptake between the defoamed and liquid samples,  
405 and three out of the eight peptides also showed significant differences in the deuterium  
406 uptake between the foam and the liquid states. Interestingly, the defoamed samples  
407 showed slower deuterium uptake than the liquid samples, which was the opposite trend  
408 to that of the foam samples (Fig. 5). This difference might be because of the aggregation  
409 induced by 90 min of foaming, and the peptides that showed significantly lower

410 deuterium uptake in the defoamed condition could be those found at the interfaces of  
411 aggregates. There is another possibility that another type of structural change, which was  
412 not detected by CD spectroscopy, could occur after defoaming. However, in either case,  
413 these results indicated that the structural changes at the foam AWI are likely to be  
414 reversible. These results emphasized the advantage of in situ structural analysis of  
415 proteins in the foam state.

416

#### 417 **Influence of hydrophobicity and surface charge**

418 The AWI is hydrophobic,<sup>1</sup> and thus the hydrophobic moieties of a protein are generally  
419 thought to adsorb to the AWI. Positively charged amino acids are also potential  
420 interaction sites with the AWI via electrostatic interactions].<sup>25</sup> The hydrophobicity and  
421 surface charge of the HSA surface were estimated using eF-site (Fig. 6).<sup>43,44</sup> The surface  
422 charge of the interacting peptides was mainly negative (shown as red in Fig. 6) and the  
423 AWI is negatively charged, which suggested that electrostatic interactions do not  
424 participate in the adsorption of HSA on the foam surface. There were some hydrophobic  
425 moieties (yellow) identified in the interacting peptides. These results suggested that  
426 hydrophobicity was the main factor for the interaction with the foam AWI. However,  
427 considering that there are other hydrophobic surfaces in the HSA molecule, other

428 important factor(s) are likely to be involved in the adsorption to the foam surface. Because  
429 the adsorption sites identified by HDX-MS were a loop region and the *N*-terminus, the  
430 flexibility to position the hydrophobic side chain toward the AWI could be a potential  
431 factor. The structural flexibility of protein molecules has been shown to be correlated  
432 with the adsorption kinetics at the AWI.<sup>3</sup>

433 The dehydration of the protein surface, which is essential for the induction of the  
434 hydrophobic effect, can also occur for hydrophilic amino acids, which causes further  
435 difficulty in identifying the protein interaction sites with the AWI.<sup>45</sup> The analysis of  
436 various other proteins using the developed method should provide information beyond  
437 the hydrophobicity to identify the interaction sites with the foam AWI.

438 In summary, we established a method using HDX-MS and analyzed the structure of  
439 HSA at the foam AWI. Using the developed method, we revealed the adsorption sites of  
440 HSA at peptide-level resolution and demonstrated that reversible structural changes  
441 occurred at the foam surface. The established method can be used to analyze the protein  
442 structure in foam in situ with minimal influence of protein aggregation at the interface.  
443 Peptides at the *N*-terminus and at a loop region, which had hydrophobic surfaces, were  
444 identified as the adsorption sites at the foam AWI. Structural changes were induced at the

445 foam AWI after more than 1 min of foaming and were observed throughout the molecule.

446 The structural changes that occurred at the foam AWI are likely to be reversible.

447 The developed method can be applied to other proteins and proteins with additives that

448 affect the foam properties. Further research using the method established here should help

449 to understand protein foaming properties at a molecular level. In addition, structural

450 assessment of proteins at the AWI by orthogonal methods is desirable in the future to

451 support the assessment by the developed HDX-MS method.

452

453

454 **Abbreviations**

455 HDX, hydrogen/deuterium exchange; MS, mass spectrometry; AWI, air-water interface;

456 HSA, human serum albumin; CD, circular dichroism; MRE, mean residue ellipticity;

457 SEC, size exclusion chromatography.

458

459 **Acknowledgement**

460 Victoria Muir, PhD, from Edanz (<https://jp.edanz.com/ac>) edited a draft of this

461 manuscript.

462

463 **Funding sources**

464 This work was supported by JSPS KAKENHI Grant Number 19K16335.

465

466 **Author contributions**

467 Conceptualization, K.E., T.T., and S.U.; Investigation, K.E., T.T., J.M., and R.T.; Data

468 curation, K.E., T.T., J.M., and R.T.; Writing – original draft, K.E., T.T., and S.U.; Writing

469 – review & editing, K.E., T.T., and S.U.; Supervision, T.T. and S.U.

470

471 **Supporting information**

472 Figures S1–S3

473 Tables S1 and S2

474

475 **References**

- 476 1. Bregnhøj, M.; Roeters, S.J.; Chatterley, A.S.; Madzharova, F.; Mertig, R.; Pedersen,  
477 J.S.; Weidner, T. Structure and Orientation of the SARS-Coronavirus-2 Spike  
478 Protein at Air-Water Interfaces. *J Phys Chem B*. **2022**, *126*(18), 3425-3430. DOI:  
479 10.1021/acs.jpccb.2c01272.
- 480 2. Rospiccio, M.; Arsiccio, A.; Winter, G.; Pisano, R. The Role of Cyclodextrins  
481 against Interface-Induced Denaturation in Pharmaceutical Formulations: A  
482 Molecular Dynamics Approach. *Mol Pharm*. **2021**, *18*(6), 2322-2333. DOI:  
483 10.1021/acs.molpharmaceut.1c00135.
- 484 3. Li, J.; Krause, M.E.; Tu, R. Protein Instability at Interfaces During Drug Product  
485 Development; Springer Nature, 2021.
- 486 4. Damodaran, S. In situ measurement of conformational changes in proteins at liquid  
487 interfaces by circular dichroism spectroscopy. *Anal Bioanal Chem*. **2003**, *376*(2),  
488 182-188. DOI: 10.1007/s00216-003-1873-6.
- 489 5. Zhao, Y.; Cieplak, M. Structural Changes in Barley Protein LTP1 Isoforms at Air-  
490 Water Interfaces. *Langmuir*. **2017**, *33*(19), 4769-4780. DOI:  
491 10.1021/acs.langmuir.7b00791.
- 492 6. Yano, Y. F.; Uruga, T.; Tanida, H.; Toyokawa, H.; Terada, Y.; Takagaki, M.;

- 493 Yamada, H. Driving force behind adsorption-induced protein unfolding: a time-  
494 resolved X-ray reflectivity study on lysozyme adsorbed at an air/water interface.  
495 *Langmuir*. **2009**, *25*(1), 32-35. DOI: 10.1021/la803235x.
- 496 7. Kizuki, S.; Wang, Z.; Torisu, T.; Yamauchi, S.; Uchiyama, S. Relationship between  
497 aggregation of therapeutic proteins and agitation parameters: Acceleration and  
498 frequency. *J Pharm Sci*. **2023**, *112*(2), 492-505. DOI: 10.1016/j.xphs.2022.09.022.
- 499 8. Huang, T.; Tu, Z. C.; Wang, H.; Shanguan, X.; Zhang, L.; Niu, P.; Sha, X. M.  
500 Promotion of foam properties of egg white protein by subcritical water pre-  
501 treatment and fish scales gelatin. *Colloids and Surfaces A: Physicochemical and*  
502 *Engineering Aspects*. **2017**, *512*, 171-177. DOI: 10.1016/j.colsurfa.2016.10.013.
- 503 9. Blasco, L.; Viñas, M.; Villa, T.G. Proteins influencing foam formation in wine and  
504 beer: the role of yeast. *Int Microbiol*. **2011**, *14*(2), 61-71. DOI:  
505 10.2436/20.1501.01.136.
- 506 10. Hill, C.; Eastoe, J. Foams: From nature to industry. *Adv Colloid Interface Sci*. **2017**,  
507 *247*, 496-513. DOI: 10.1016/j.cis.2017.05.013.
- 508 11. Chang, Kefei.; Liu, Jingbo.; Jiang, Wei.; Fan, Yong.; Nan, Bo.; Ma, Sitong.; Zhang,  
509 Yan.; Liu, Boqun.; Zhang, Ting. Structural characteristics and foaming properties  
510 of ovalbumin - Caffeic acid complex. *LWT*. **2021**, *146*:111383. DOI:  
511 10.1016/j.lwt.2021.111383.
- 512 12. Dai, T.; McClements, D. J.; Hu, T.; Chen, J.; He, X.; Liu, C.; Sheng, J.; Sun, J.  
513 Improving foam performance using colloidal protein-polyphenol complexes:  
514 Lactoferrin and tannic acid. *Food Chem*. **2022**, *377*:131950. DOI:  
515 10.1016/j.foodchem.2021.131950.
- 516 13. Sun, J.; Chang, C.; Su, Y.; Gu, L.; Yang, Y.; Li, J. Impact of saccharides on the

- 517 foam properties of egg white: Correlation between rheological, interfacial  
518 properties and foam properties. *Food Hydrocolloids*. **2021**, *122*:107088. DOI:  
519 10.1016/j.foodhyd.2021.107088.
- 520 14. Duan, X.; Li, M.; Shao, J.; Chen, H.; Xu, X.; Jin, Z.; Liu, X. Effect of oxidative  
521 modification on structural and foaming properties of egg white protein. *Food*  
522 *Hydrocolloids*. **2018**, *75*:223-228. DOI: 10.1016/j.foodhyd.2017.08.008.
- 523 15. Sun, L.; Wu, Q.; Mao, X. Effects of Oxidation Modification by Malondialdehyde  
524 on the Structure and Functional Properties of Walnut Protein. *Foods*. **2022**,  
525 *11*(16):2432. DOI: 10.3390/foods11162432.
- 526 16. Perriman, A. W.; Henderson, M. J.; Evenhuis, C. R.; McGillivray, D. J.; White, J.  
527 W. Effect of the air-water interface on the structure of lysozyme in the presence of  
528 guanidinium chloride. *J Phys Chem B*. **2008**, *112*(31):9532-9. DOI:  
529 10.1021/jp800354r.
- 530 17. Hamuro, Y. Tutorial: Chemistry of Hydrogen/Deuterium Exchange Mass  
531 Spectrometry. *J Am Soc Mass Spectrom*. **2021**, *32*(1):133-151. DOI:  
532 10.1021/jasms.0c00260.
- 533 18. Weis D. D. Hydrogen Exchange Mass Spectrometry of Proteins: Fundamentals,  
534 Methods, and Applications; Wiley, 2016.
- 535 19. Kheterpal, I.; Wetzel, R. Hydrogen/deuterium exchange mass spectrometry--a  
536 window into amyloid structure. *Acc Chem Res*. **2006**, *39*(9), 584-93. DOI:  
537 10.1021/ar050057w.
- 538 20. Brown, K. A.; Wilson, D. J. Bottom-up hydrogen deuterium exchange mass  
539 spectrometry: data analysis and interpretation. *Analyst*. **2017**, *142*(16):2874-2886.  
540 DOI: 10.1039/c7an00662d.

- 541 21. Buijs, J.; Costa Vera, C.; Ayala, E.; Steensma, E.; Håkansson, P.; Oscarsson, S.  
542 Conformational stability of adsorbed insulin studied with mass spectrometry and  
543 hydrogen exchange. *Anal Chem.* **1999**, *71*(15):3219-25. DOI: 10.1021/ac9809433.
- 544 22. Buijs, J.; Speidel, M.; Oscarsson, S. The Stability of Lysozyme Adsorbed on Silica  
545 and Gallium Arsenide Surfaces: Preferential Destabilization of Part of the  
546 Lysozyme Structure by Gallium Arsenide. *Journal of Colloid and Interface  
547 Science.* **2000**, *226*(2):237-245. DOI: 10.1006/jcis.2000.6818.
- 548 23. Buijs, J.; Ramström, M.; Danfelter, M.; Larsericsdotter, H.; Håkansson, P.;  
549 Oscarsson, S. Localized changes in the structural stability of myoglobin upon  
550 adsorption onto silica particles, as studied with hydrogen/deuterium exchange mass  
551 spectrometry. *J Colloid Interface Sci.* **2003**, *263*(2):441-8. DOI: 10.1016/s0021-  
552 9797(03)00401-6.
- 553 24. Xiao, Y.; Konermann, L. Protein structural dynamics at the gas/water interface  
554 examined by hydrogen exchange mass spectrometry. *Protein Sci.* **2015**, *24*(8):1247-  
555 56. DOI: 10.1002/pro.2680.
- 556 25. Han, F.; Shen, Q.; Zheng, W.; Zuo, J.; Zhu, X.; Li, J.; Peng, C.; Li, B.; Chen, Y.  
557 The Conformational Changes of Bovine Serum Albumin at the Air/Water Interface:  
558 HDX-MS and Interfacial Rheology Analysis. *Foods.* **2023**, *12*(8):1601. DOI:  
559 10.3390/foods12081601.
- 560 26. Ascenzi, P.; di Masi, A.; Fanali, G.; Fasano, M. Heme-based catalytic properties of  
561 human serum albumin. *Cell Death Discov.* **2015**, *1*:15025. DOI:  
562 10.1038/cddiscovery.2015.25.
- 563 27. Jahanban-Esfahlan, A.; Ostadrahimi, A.; Jahanban-Esfahlan, R.; Roufegarinejad,  
564 L.; Tabibiazar, M.; Amarowicz, R. Recent developments in the detection of bovine

- 565 serum albumin. *Int J Biol Macromol.* **2019**, *138*:602-617. DOI:  
566 10.1016/j.ijbiomac.2019.07.096.
- 567 28. Zhou, L.; Luo, M.; Tian, R.; Zeng, X. P.; Peng, Y. Y.; Lu, N. Generation of a  
568 Bovine Serum Albumin-Diligand Complex for the Protection of Bioactive  
569 Quercetin and Suppression of Heme Toxicity. *Chem Res Toxicol.* **2021**, *34*(3):920-  
570 928. DOI: 10.1021/acs.chemrestox.0c00537.
- 571 29. Chen, Z.; Zhong, M.; Luo, Y.; Deng, L.; Hu, Z.; Song, Y. Determination of  
572 rheology and surface tension of airway surface liquid: a review of clinical relevance  
573 and measurement techniques. *Respir Res.* **2019**, *20*(1):274. DOI: 10.1186/s12931-  
574 019-1229-1.
- 575 30. Berry, J. D.; Neeson, M. J.; Dagastine, R. R.; Chan, D. Y.; Tabor, R. F.  
576 Measurement of surface and interfacial tension using pendant drop tensiometry. *J*  
577 *Colloid Interface Sci.* **2015**, *454*:226-37. DOI: 10.1016/j.jcis.2015.05.012.
- 578 31. Anthis, N. J.; Clore, G. M. Sequence-specific determination of protein and peptide  
579 concentrations by absorbance at 205 nm. *Protein Sci.* **2013**, *22*(6):851-8. DOI:  
580 10.1002/pro.2253.
- 581 32. Micsonai, A.; Wien, F.; Kernya, L.; Lee, Y. H.; Goto, Y.; Réfrégiers, M.; Kardos, J.  
582 Accurate secondary structure prediction and fold recognition for circular dichroism  
583 spectroscopy. *Proc Natl Acad Sci U S A.* **2015**, *112*(24):E3095-103. DOI:  
584 10.1073/pnas.1500851112.
- 585 33. Glasoe, P. K., Long, F. A. Use of glass electrodes to measure acidities in deuterium  
586 oxide. *Journal of Physical Chemistry.* **1960**, *64*:188-189. DOI:  
587 10.1021/j100830a521.
- 588 34. Weis, D. D. Recommendations for the Propagation of Uncertainty in Hydrogen

- 589 Exchange-Mass Spectrometric Measurements. *J. Am. Soc. Mass Spectrom.* **2021**,  
590 32, 1610, DOI: 10.1021/jasms.0c00475.
- 591 35. Hageman, T. S.; Weis, D. D. Reliable Identification of Significant Differences in  
592 Differential Hydrogen Exchange-Mass Spectrometry Measurements Using a  
593 Hybrid Significance Testing Approach. *Anal Chem.* **2019**, *91*(13):8008-8016. DOI:  
594 10.1021/acs.analchem.9b01325.
- 595 36. Leiske, D. L.; Shieh, I. C.; Tse, M. L. A Method To Measure Protein Unfolding at  
596 an Air-Liquid Interface. *Langmuir.* **2016**, *32*(39):9930-9937. DOI:  
597 10.1021/acs.langmuir.6b02267.
- 598 37. Duerkop, M.; Berger, E.; Dürauer, A.; Jungbauer, A. Impact of Cavitation, High  
599 Shear Stress and Air/Liquid Interfaces on Protein Aggregation. *Biotechnol J.* **2018**,  
600 *13*(7):e1800062. DOI: 10.1002/biot.201800062.
- 601 38. Masson, G. R.; Burke, J. E.; Ahn, N. G.; Anand, G. S.; Borchers, C.; Brier, S.; Bou-  
602 Assaf, G.M.; Engen, J.R.; Englander, S.W.; Faber, J.; et al. Recommendations for  
603 performing, interpreting and reporting hydrogen deuterium exchange mass  
604 spectrometry (HDX-MS) experiments. *Nat Methods.* **2019**, *16*(7):595-602. DOI:  
605 10.1038/s41592-019-0459-y.
- 606 39. Peacock, R. B.; Komives, E. A. Hydrogen/Deuterium Exchange and Nuclear  
607 Magnetic Resonance Spectroscopy Reveal Dynamic Allostery on Multiple Time  
608 Scales in the Serine Protease Thrombin. *Biochemistry.* **2021**, *60*(46):3441-3448.  
609 DOI: 10.1021/acs.biochem.1c00277.
- 610 40. Narang, D.; Lento, C.; Wilson, J. HDX-MS: An Analytical Tool to Capture Protein  
611 Motion in Action. *Biomedicines.* **2020**, *8*(7):224. DOI:  
612 10.3390/biomedicines8070224.

- 613 41. Chalmers, M. J.; Busby, S. A.; Pascal, B. D.; West, G. M.; Griffin, P. R.  
614 Differential hydrogen/deuterium exchange mass spectrometry analysis of protein-  
615 ligand interactions. *Expert Rev Proteomics*. **2011**, *8*(1):43-59. DOI:  
616 10.1586/epr.10.109.
- 617 42. Rogóż, W.; Lemańska, O.; Pożycka, J.; Owczarzy, A.; Kulig, K.; Muhammetoglu,  
618 T.; Maciążek-Jurczyk, M. Spectroscopic Analysis of an Antimalarial Drug's  
619 (Quinine) Influence on Human Serum Albumin Reduction and Antioxidant  
620 Potential. *Molecules*. **2022**, *27*(18):6027. DOI: 10.3390/molecules27186027.
- 621 43. Yano, Y. F.; Arakawa, E.; Voegeli, W.; Kamezawa, C.; Matsushita, T. Initial  
622 Conformation of Adsorbed Proteins at an Air-Water Interface. *J Phys Chem B*.  
623 **2018**, *122*(17):4662-4666. DOI: 10.1021/acs.jpcc.8b01039.
- 624 44. Kinoshita, K.; Furui, J.; Nakamura, H. Identification of protein functions from a  
625 molecular surface database, eF-site. *J Struct Funct Genomics*. **2002**, *2*(1):9-22.  
626 DOI: 10.1023/a:1011318527094.
- 627 45. Rego, N. B.; Xi, E.; Patel, A. J. Identifying hydrophobic protein patches to inform  
628 protein interaction interfaces. *Proc Natl Acad Sci U S A*. **2021**,  
629 *118*(6):e2018234118. DOI: 10.1073/pnas.2018234118.
- 630

631 **Figures captions:**

632

633 **Figure 1.** (a) Adsorption of HSA at the AWI evaluated by interfacial tension  
634 measurement. The dashed line represents the static surface tension measured by the  
635 Whilhelmy method [ $50.6 \pm 0.16$  (HSA solution) and  $70.8 \pm 0.05$  mN/m (phosphate  
636 buffer)] and the dots are the results of dynamic surface tension measurements. (b) HSA  
637 solution (left) was foamed using a milk frother (right).

638

639 **Figure 2.** SEC after foaming. (a) The time course of the total peak area of monomer and  
640 aggregates are shown as gray bars and the time course of the monomer percentage is  
641 also plotted. Error bars represent the SD of three measurements. The asterisk indicates  
642 the statistical difference in monomer% tested by the Dunnett's test ( $p < 0.01$ ). (b) A  
643 representative chromatogram before foaming (0 min) and after foaming (90 min).

644

645 **Figure 3.** HDX-MS results for foam samples. (a) Deuterium uptake plots of peptides  
646 that showed significant differences between the foam and liquid samples. The  
647 deuterium uptake was calculated by subtracting the centroid mass at  $t = 0$  from the  
648 centroid mass at each time point. The asterisk denotes a statistically significant

649 difference. (b) The peptides that showed significantly lower deuterium uptake at 1 min  
650 in the foam state are colored cyan and (c) the peptides that showed significantly higher  
651 deuterium uptake at 90 min are colored magenta.

652

653 **Figure 4.** CD spectra of defoamed samples. The secondary structure composition  
654 calculated by BeStSel is shown below the spectra.

655

656 **Figure 5.** HDX-MS results for defoamed samples. (a) Deuterium uptake plots of  
657 peptides that showed significant differences between the defoamed and liquid samples.  
658 (b) The peptides that showed significantly lower deuterium uptake at 90 min in the  
659 defoamed state are colored green.

660

661 **Figure 6.** (a) Surface charge and hydrophobicity of HSA calculated using eF-site.  
662 Positively and negatively charged surfaces are colored blue and red, respectively.  
663 Magnified view of peptides A2-F19 (b) and E492-T506 (c).

664